Numerical studies of a three-dimensional flow in suddenly contracted channels

T. P. Chiang and Tony W. H. Sheu[a)]
Department of Engineering Science and Ocean Engineering, National Taiwan University, Taipei, Taiwan, Republic of China

Robert R. Hwang
Institute of Physics, Academia Sinica, Taipei, Taiwan, Republic of China

(Received 22 October 2001; accepted 18 January 2002; published 19 March 2002)

This paper aims to provide deeper insight into the suddenly contracted channel flow. The channels under investigation have a width of $18D$, where D represents the channel height upstream of the step plane, and two contraction ratios: $C=2$ and 4. In the present three-dimensional finite volume analysis, the advective fluxes are discretized using an upwind scheme that provides a third-order accurate solution in uniform grid cases. For efficient calculation of field variables, working equations are solved separately based on the semi-implicit velocity-pressure coupling procedures. We exploit a theoretically appealing topological theory to determine lines of separation and reattachment, from which the pitchfork bifurcation flow can be identified in the contraction channel. To further elucidate the vortical details of the channel flow, we trace massless particles seeded in the flow, showing the spanwise spiraling flow motion. Emphasis is placed on flow phenomena in the upstream salient corner eddy and downstream tip corner eddy. © *2002 American Institute of Physics.* [DOI: 10.1063/1.1459719]

I. INTRODUCTION

There are many cases in which flow phenomenon downstream of a suddenly contracted channel is important, with the non-Newtonian flow case being of particular interest. The practical importance in the polymer processing industries (Crochet *et al.*[1]) has prompted extensive investigations. The flow geometry we consider in this simulation is that of an idealized suddenly contracted channel. The step plane is considered to be normal to the direction of the channel walls. This flow has been investigated experimentally (see, for example, Durst *et al.*[2]). Numerical investigations into the problem of present interest have been quite plentiful. However, they were mostly conducted on a two-dimensional basis (Dennis and Smith,[3] Hunt,[4] Hawken *et al.*,[5] Huang and Seymour,[6] and Chiang and Sheu[7]).

Separation in a contraction channel can be characterized by the recirculation eddies at the upstream salient corner and downstream tip corner as shown in Fig. 1. The separation length L_1 and the reattachment length L_2 of the upstream salient corner eddy were reported to decrease in their magnitudes as the Reynolds number Re is increased from zero.[2–7] These values become increasing when $Re>100$ (Ref. 6). As $Re>1000$, L_1 follows the asymptotic formula $L_1=(0.1289^{*}\ln(Re/2)-0.5365)/2$ for the channel with contraction ratio $C=2$ (Ref. 3). Hawken *et al.*[5] revealed that the downstream tip corner eddy becomes visible in the range of $300<Re<500$ and $200<Re<300$ for $C=2$, and 4, respectively, and, becomes larger as Re increases. The reattachment length L_3 varies linearly with the Reynolds number Re according to $L_3=a^{*}Re-b$, where (a, b) are estimated to be $(0.3364\times10^{-3},0.1088)$ and $(0.4011\times10^{-3},0.0565)$ for $C=2$ $(500\leqslant Re\leqslant 4000)$ and 4 $(300\leqslant Re\leqslant 2000)$, respectively.[7]

Considering the rapidly increasing use of computational fluid dynamics code to model flow behavior, we performed in this study a three-dimensional simulation to investigate the effects of the Reynolds numbers and the contraction ratios on the contraction channel flow. As a first attempt to study this problem, we considered a channel used in an experimental work so as to reproduce experimental measurements[2] and, thus, validate the analysis code. Another aim was to provide further details about the nature of the flow that was difficult to obtain in the experiment.

When considering the flow downstream of a planar and symmetric channel expansion, a larger re-circulating region, which appeared preferentially at one wall of the channel, was experimentally observed by Cherdron *et al.*[8] and Sobey.[9] Above the critical Reynolds number, Re_c, the flow pattern becomes substantially different from that observed below this value. Under these circumstances, the suddenly expanded flow can no longer be symmetric about the centerline of the channel, and a process known as pitchfork bifurcation can occur. This causes momentum transfer to proceed between the fluid shear layers and can, in turn, cause a pressure of nonuniform type to form across the channel. This established pressure gradient leads to an asymmetric flow, which we refer to as the Coanda effect (Wille and Fernolz[10]). Investigations into the flow asymmetry in a geometrically symmetric channel have mostly focused on flow through planar

[a)]Author to whom correspondence should be addressed. Telephone: 886-2-23625470 ext. 246; fax: 886-2-23661703; electronic mail: sheu@sccs.na.ntu.edu.tw

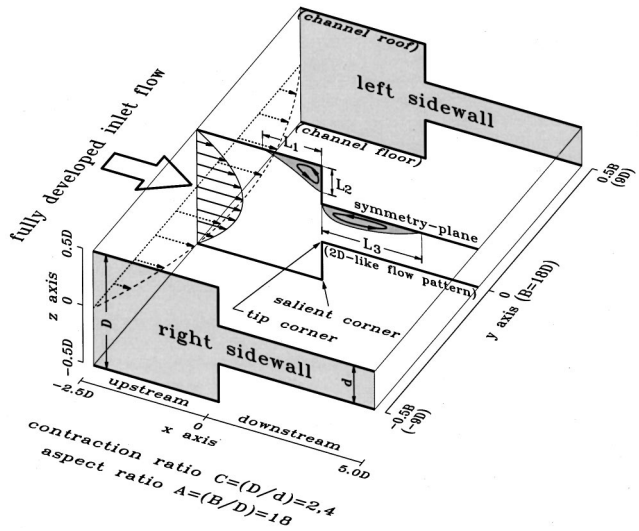

FIG. 1. Schematic of the three-dimensional channel, with a suddenly contracted plane at $x=0$. Both separated–reattached lengths and boundary conditions are provided.

symmetric channel expansions. One can refer to the works of Fearn *et al.*,[11] Drikakis,[12] Battaglia *et al.*,[13] Alleborn *et al.*,[14] Rusak and Hawa,[15] Mizushima and Shiotani,[16] and Hawa and Rusak,[17,18] which provided clear insight into the flow dynamics near the critical Reynolds number and demonstrated the existence of a bifurcation phenomenon.

Previous numerical studies[2–6] have conducted the two-dimensional contraction flow analyses only in the half-channel. The present authors presented the critical Reynolds numbers as 3075 and 1355 in their two-dimensional full-channel calculations for $C=2$ and 4, respectively.[7] To the best of authors' knowledge, no investigation has been conducted to study the bifurcation flow in the three-dimensional sudden contraction channel. The present three-dimensional study takes the channel span into consideration. One of our main aims is to determine whether pitchfork bifurcation remains a main signature of the three-dimensional flow in the contraction channel.

The remaining sections of this paper are organized as follows. In Sec. II, we present equations that govern the flow motion in the channel. This is followed by a brief introduction to the finite volume discretization method and the segregated solution algorithm. Section IV is devoted to describing first the investigated problem and, then, the validation study of the employed analysis code. In Sec. V, we present numerical results obtained at two contraction ratios and five Reynolds numbers. To broaden our understanding of the flow separation–reattachment in the channel, we adopt a theoretically rigorous topological theory. We show that three-dimensional pitchfork bifurcation is physically relevant and can be suppressed as the channel aspect ratio is reduced. We also study in detail the spanwise spiraling flow structure inside the salient and tip eddies. Finally, we provide in Sec. VI concluding remarks.

II. MATHEMATICAL MODEL

In the present investigation, the numerical technique was used to simulate the three-dimensional steady incompressible and viscous flow of a non-conducting fluid through a contraction channel schematically shown in Fig. 1. The Newtonian fluid under investigation has a constant dynamic viscosity. The governing equations that can describe the contraction channel flow motion are expressed in vector form as

$$\underline{u}\cdot\nabla\underline{u}=-\nabla p+\frac{1}{Re}\nabla^2\underline{u}, \tag{1}$$

$$\nabla\cdot\underline{u}=0. \tag{2}$$

In the above primitive-variable equations, u, v, and w are the velocity components in the x, y, and z directions, respectively, and p is the static fluid pressure. All the variables have been normalized by dividing the velocity components by the chosen characteristic velocity U_{char}, which takes on a value 2/3 times that of the inlet maximum velocity $u_{\max}(\equiv 3/2)$, and by the pressure by ρU_{char}^2, where ρ is the fluid density. All the independent variables are nondimensionalized by the upstream channel height $D(\equiv 1)$, leading to a Reynolds number of $Re=(\frac{3}{2}u_{\text{mean}})(D)/\mu$, where μ denotes the dynamic viscosity of the fluid.

TABLE I. Separation and reattachment lengths for the case of $C=2$ and grid details used in the grid independent tests (2D, half-domain computation).

Length	L_1		L_2		L_3	
Reynolds number *Re*	1000	2000	1000	2000	1000	2000
Dennis and Smith (Ref. 3)	0.1375	0.1819	0.0808	0.0926	⋯	⋯
Hunt (Ref. 4)	0.1540	0.1970	0.0820	0.0940	0.2070	0.4805
Hawken *et al.* (Ref. 5)	0.1425	⋯	0.0770	⋯	0.2388	⋯
Huang and Seymour (Ref. 6)	0.1375	⋯	0.0805	⋯	0.2220	⋯
Present:[a] $h=1/20$	0.0847	0.1448	0.0561	0.0667	none	none
1/40	0.1619	0.2015	0.0812	0.0927	0.1816	0.3445
1/80	0.1521	0.1977	0.0835	0.0943	0.2538	0.6385
1/160	0.1459	0.1912	0.0834	0.0945	0.2687	0.6058
1/320	0.1419	0.1862	0.0825	0.0941	0.2347	0.5677
1/640	0.1397	0.1831	0.0819	0.0936	0.2222	0.5431
1/1280	0.1386	0.1815	0.0816	0.0934	0.2199	0.5350

[a] $x(\min,\max)=(-1.0,1.0)$.

TABLE II. Grid details of the nonuniform Grid-A ($A=18$).

C	x(min,max)	$N(dx,dy,dz)$	dx(min,max)	dy(min,max)	dz(min,max)
2	(−2.5, 5.0)	(110, 100, 130)	(0.001, 0.25)	(0.01, 0.48)	(0.0005, 0.02)
4	(−2.5, 5.0)	(110, 100, 180)	(0.001, 0.25)	(0.01, 0.48)	(0.0005, 0.01)

We favor the primitive-variable formulation owing to its accommodation of closure boundary conditions (Ladyzhenskaya[19]). In all the cases investigated, the same parabolic velocity profile (Fig. 1) was specified at each channel inlet. As with many other inflow–outflow simulations, the flow at the channel exit was assumed to have a zero gradient in the axial direction. The rate of change of both velocity components remains unchanged with the distance along the channel. The no-slip and no-penetration conditions are used along the channel walls. The presently employed primitive-variable formulation can avoid dealing with the sharp corner singularity (infinite vortivity at the downstream tip corner), which will be a difficult problem to deal with when using the stream function-vorticity formulation.[3,4,6]

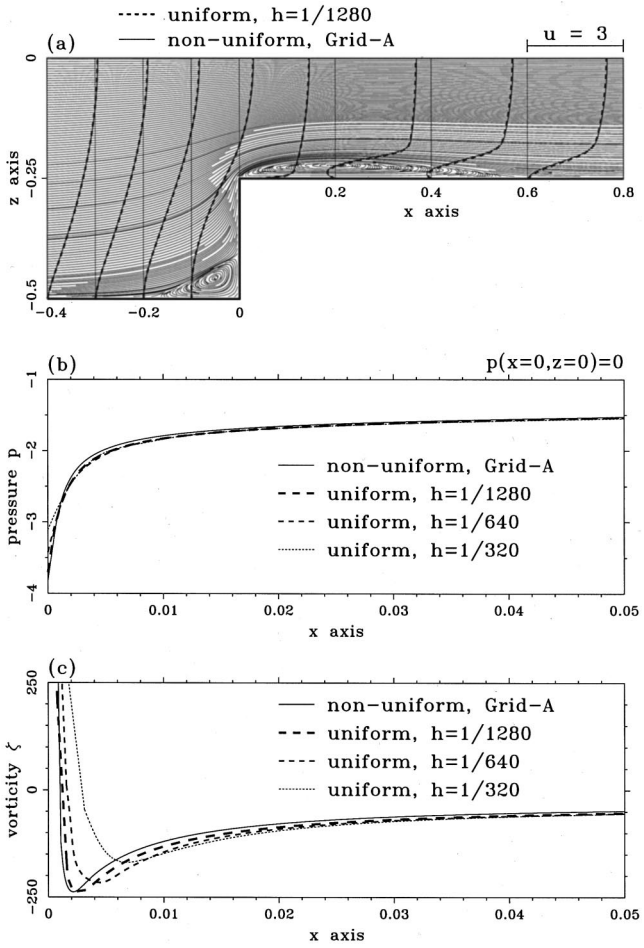

FIG. 2. Comparison of computed results under uniform and nonuniform grids in a two-dimensional channel with $C=2$ and $Re=2000$. (a) Streamwise velocity profiles; (b) pressure distribution along the downstream channel roof–floor; (c) vorticity distribution along the downstream channel roof–floor.

III. NUMERICAL MODEL

In solving the primitive-variable equations (1) and (2), together with the above-mentioned boundary conditions, we employ a finite volume discretization method. A serious problem worthy of consideration is that solutions to incompressible Navier–Stokes equations are prone to checkerboard pressure oscillations. To circumvent this difficulty, field variables are stored on staggered, interconnected grids. Following the standard finite volume method, working equations are integrated in their respective control volumes, each of which is associated with its representative primitive variable and is placed on the centroid of the control volume.

Numerical simulation of incompressible Navier–Stokes equations leads to the convective instability problem. Physically erroneous oscillatory velocities occur when dominating advective terms are discretized using centered schemes. This can result in numerical instability, which is particularly severe in multidimensional flow simulations. To fix this problem, we have modified the QUICK scheme (third-order accuracy) of Leonard[20] and implemented it on nonuniform grids. This modification not only resolves the convective in-

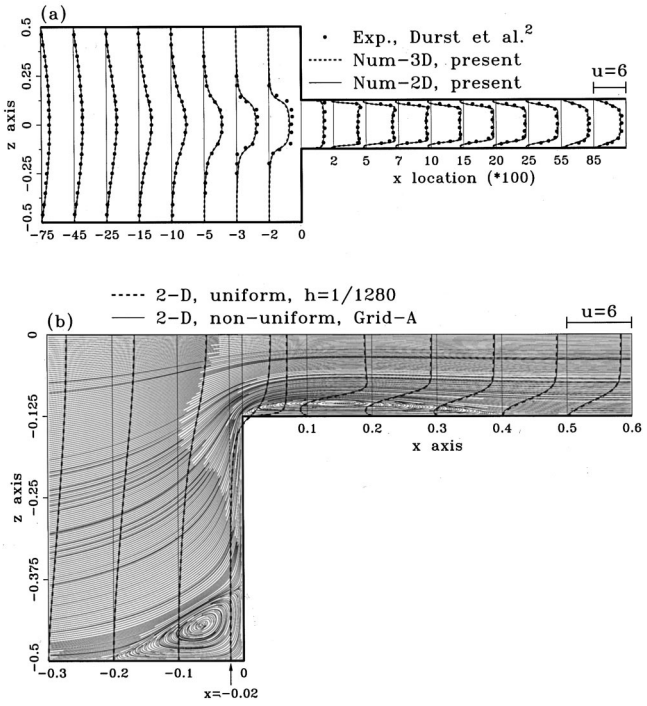

FIG. 3. (a) Comparison of the computed two- and three-dimensional streamwise velocity profiles at the plane of symmetry, $y=0$, with the experimental data of Durst *et al.* (Ref. 2) for the case with $C=4$ and $Re=1150$; (b) comparison of the streamwise velocity profiles computed under the uniform and nonuniform grids in a two-dimensional channel with $C=4$ and $Re=1150$.

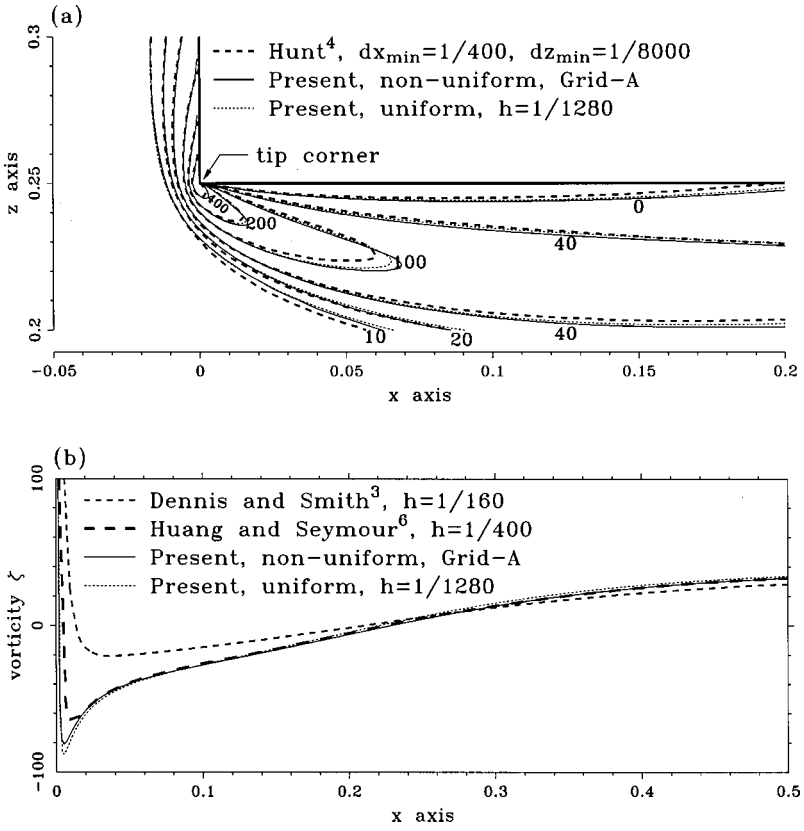

FIG. 4. Comparison of the computed vorticity with that using the stream function-vorticity formulation in a two-dimensional channel with $C=2$ and $Re=1000$. (a) Vorticity contours near the tip corner; (b) vorticity distribution along the downstream channel roof–floor.

stability problem, but also improves the prediction accuracy. Discretization of other spatial derivatives is performed using the centered-scheme (second-order accuracy) for physical reasons. For a more detailed representation of the nonuniform flux discretization, see for example Chiang *et al.*[21]

When solving the finite volume discretized equations for (1) and (2), we abandon the mixed formulation due to the need for a much more disk storage space compared to the

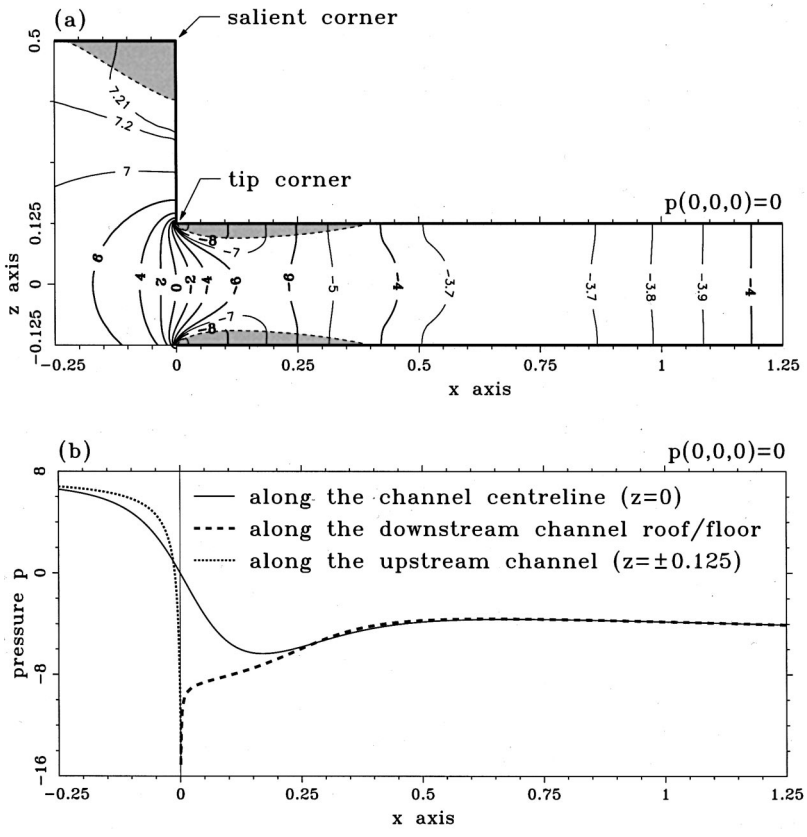

FIG. 5. Pressure for the case with $C=4$, $A=18$, and $Re=1150$. (a) Pressure contours on the plane of symmetry $y=0$; (b) the distribution of $p(x,0,0)$ and $p(x,0,\pm 0.125)$.

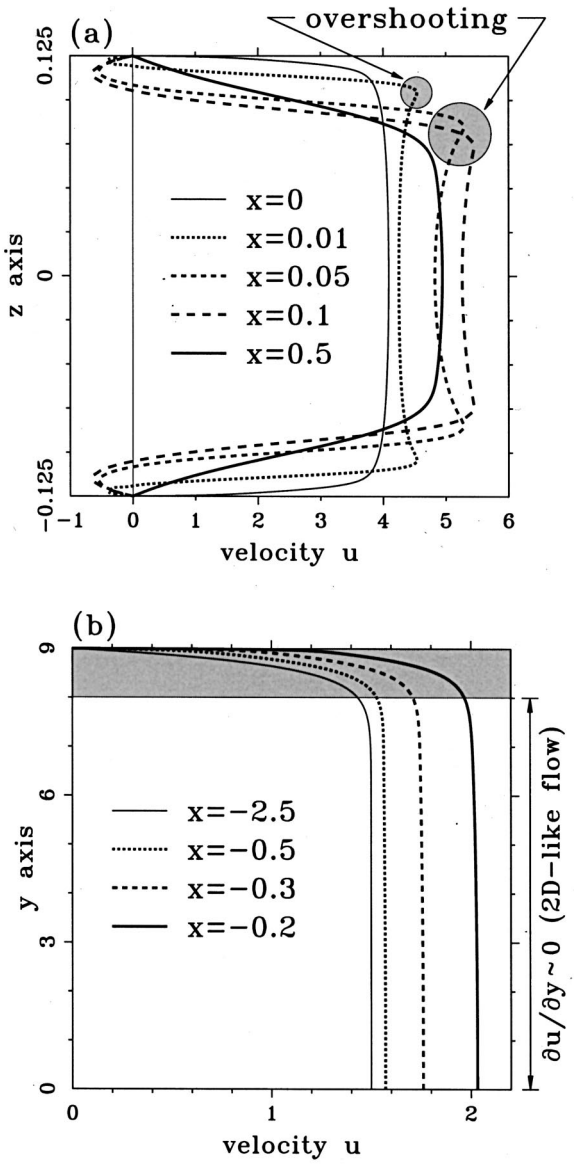

FIG. 6. Velocity profiles for the case with $C=4$, $A=18$, and $Re=1150$. (a) $u(z)$ downstream of the contracted plane at the plane of symmetry $y=0$; (b) $u(y)$ upstream of the contracted plane at the plane of symmetry $z=0$.

space needed when using a segregated approach. Of the segregated approaches available in the literature, we adopt the SIMPLE-C solution algorithm of Van Doormaal and Raithby[22] as it has been shown to have the ability to produce

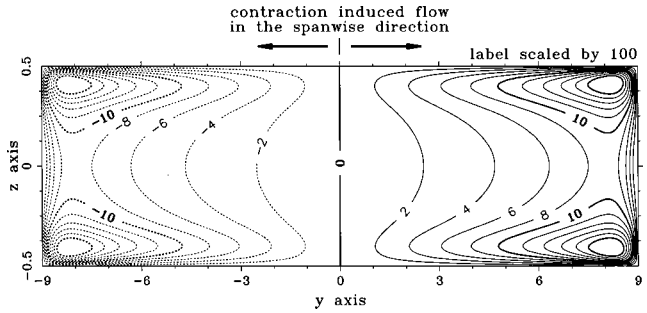

FIG. 7. A contour plot of v at the plane $x=-0.5$ for the case with $C=4$, $A=18$, and $Re=1150$ to illustrate the spanwise flow motion.

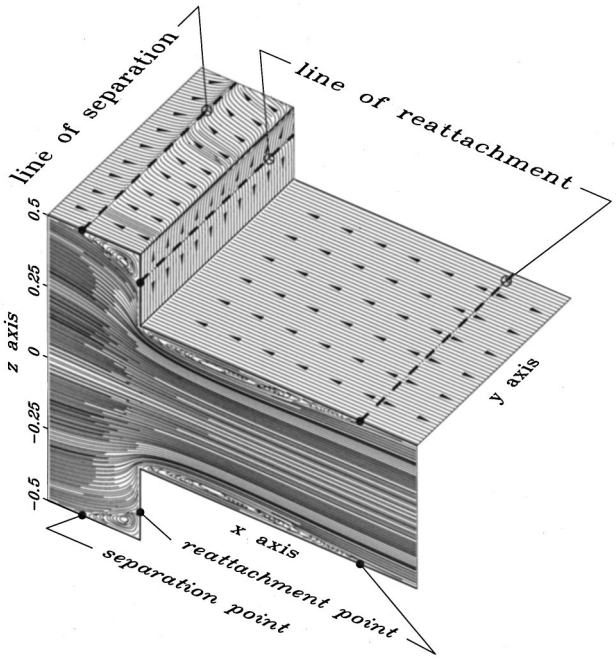

FIG. 8. Lines of separation and reattachment on the channel roof for the case with $C=2$ and $Re=2500$.

accurate results at a good rate of convergence. The pressure field is solved using the pressure-velocity coupling method and the mass continuity equation (2). In the staggered meshes, there are no storage points for the pressure at the domain boundary. As a result, specification of pressure

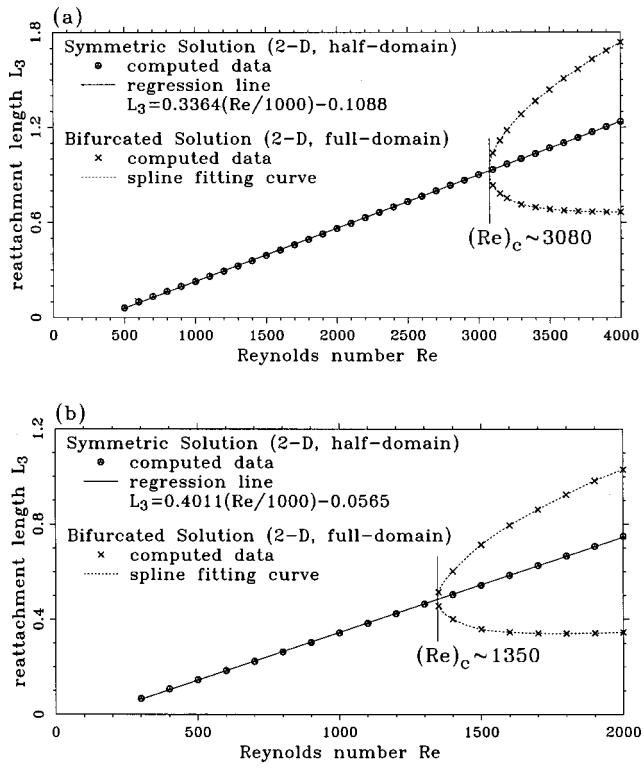

FIG. 9. Numerical bifurcation diagram obtained from the simulated reattachment lengths of the downstream tip corner eddy. (a) $C=2$; (b) $C=4$ [from Chiang and Sheu (Ref. 7)].

TABLE III. Separation and reattachment lengths (Grid-A, full-domain computation).

C	Re	2-, or 3[a]-dimension	L_1 (roof, floor)	L_2 (roof, floor)	L_3 (roof, floor)
2	426	2	(0.098, 0.098)	(0.067, 0.067)	(none, none)
		3	(0.100, 0.100)	(0.068, 0.068)	(none, none)
	2500	2	(0.196, 0.197)	(0.093, 0.093)	(0.731, 0.738)
		3	(0.207, 0.207)	(0.098, 0.098)	(0.715, 0.722)
	3150	2	(0.210, 0.212)	(0.097, 0.099)	(0.783, 1.117)
		3	(0.223, 0.225)	(0.102, 0.102)	(0.835, 1.037)
4	1150	2	(0.212, 0.212)	(0.115, 0.115)	(0.401, 0.406)
		3	(0.229, 0.229)	(0.124, 0.124)	(0.391, 0.396)
	1500	2	(0.230, 0.232)	(0.120, 0.122)	(0.358, 0.714)
		3	(0.250, 0.252)	(0.132, 0.133)	(0.365, 0.684)

[a]Aspect ratio $A=18$, on the symmetry-plane $y=0$.

boundary conditions is not needed. The scheme adopted here has been validated against the analytic scalar transport equation and Navier–Stokes equations to ensure its spatial accuracy. The interested reader can refer to Chiang and Sheu.[23] In all the cases investigated, the solution was considered to have converged when the global L_2-norms of pressure and velocity residuals all dropped by at least ten orders of magnitude. Besides imposing this stringent convergence requirement, it is also demanded that the relative difference of the mass flux between the inlet and other arbitrarily chosen sections be less than 10^{-10}.

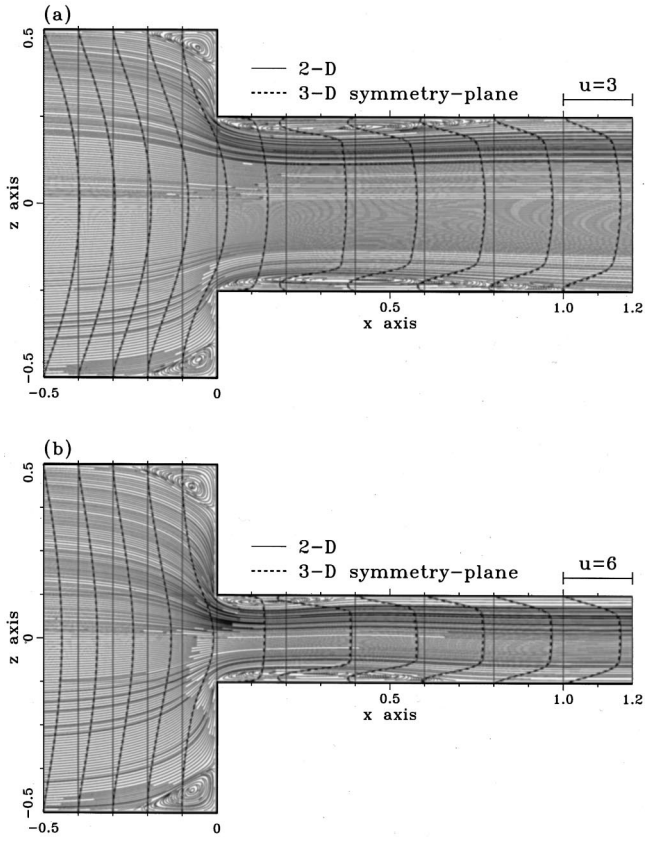

FIG. 10. Streamwise velocity distributions and pseudo streamlines on the plane of symmetry $y=0$ for showing the presence of a pitchfork bifurcation solution. (a) $C=2$, $A=18$, and $Re=3150$; (b) $C=4$, $A=18$, and $Re=1500$.

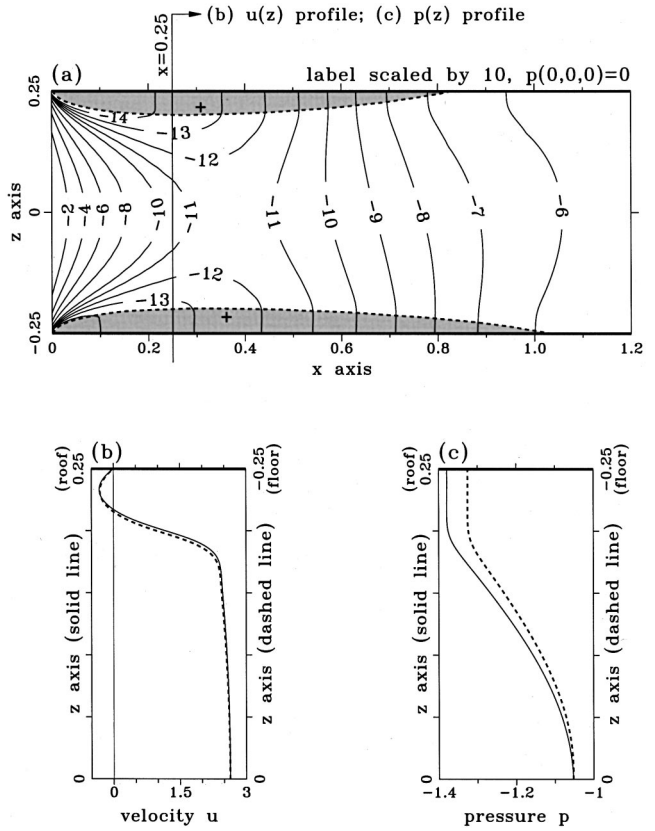

FIG. 11. The three-dimensional computed solutions for the case with $C=2$, $A=18$, and $Re=3150$. (a) Pressure contour on the plane of symmetry $y=0$; (b) velocity profile $u(0.25,0,z)$; (c) pressure profile $p(0.25,0,z)$.

IV. PROBLEM DESCRIPTION AND CODE VALIDATION

The Cartesian coordinate system, with the origin located at the contraction plane, used for the three-dimensional study is depicted in Fig. 1. The x direction is defined as being the direction of the bulk of the fluid flow. The y and z coordinates represent the spanwise and step-height directions, respectively. The upstream channel height and the step height are $D(\equiv 1)$ and $\frac{1}{2}(D-d)$, respectively. The channel height downstream of the contraction is d, leading to a contraction ratio of $C(\equiv D/d)$. Upstream of the step plane, the flow enters the channel at $x=-2.5D$, at which point a fully developed velocity profile (White[24]) having a maximum value of 3/2 is prescribed. In this study, we consider that the channel exit is truncated far downstream of the step to allow the flow to have a negligibly small velocity gradient: Given this assumption, we prescribe a zero gradient velocity vector in the axial direction at $x=5D$ to close the problem. In the present investigation, computer code was run to simulate the fluid flow through channels with a width of $18D$ (Ref. 2), each of which contained a planar symmetric contraction at $x=0$. The channel geometry was characterized by the contraction ratio. The Reynolds numbers investigated were 426, 2500, and 3150 for the case of $C=2$, and 1150 and 1500 for the case of $C=4$.

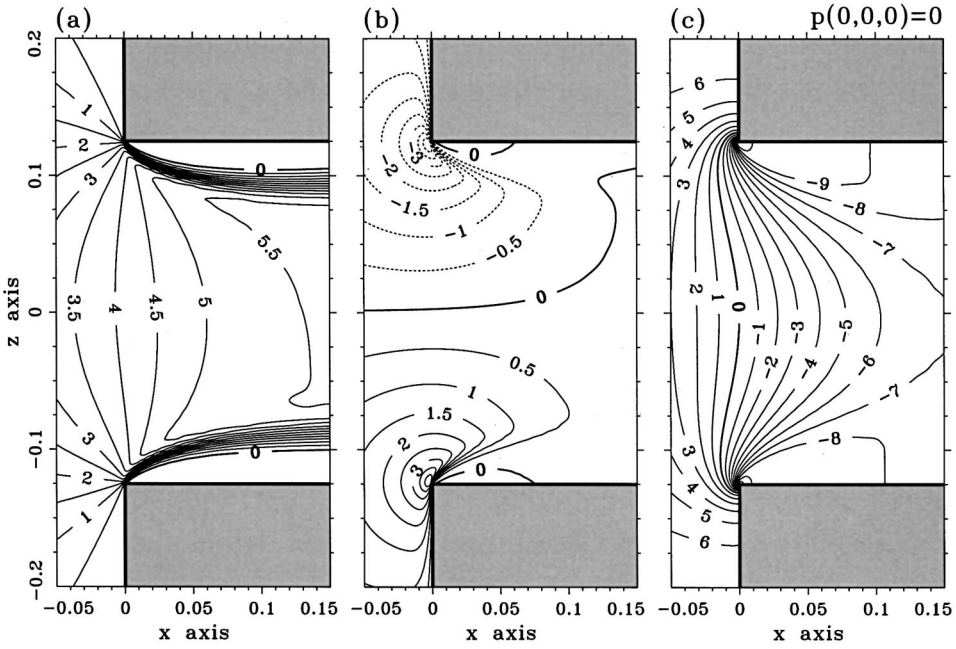

FIG. 12. The computed contours on the plane of symmetry $y=0$ near the contraction step for the case of $C=4$, $A=18$, and $Re=1500$. (a) u-contours; (b) w-contours; (c) p contours.

As is normally the case when conducting a numerical flow simulation, we performed grid-independent tests. To conduct these tests, Cartesian grids were overlaid uniformly in the two-dimensional channel with $C=2$ at $Re=1000$ and 2000. As Table I shows, the results computed at seven investigated grids provided grid-independent solutions in the sense that one separation length (L_1 schematically shown in Fig. 1) and two reattachment lengths (L_2 and L_3 schematically shown in Fig. 1) all differed by less than 1.5% for the two finest test grids, $h=1/640$ and 1/1280.

Prior to demonstrating the integrity of the code, it is important to justify the rationale behind using nonuniform grids in the subsequent three-dimensional calculations. From the physical point of view, grids should be packed in regions where the boundary layer effect prevails. The nonuniform grid Grid-A ($dx_{\min}=1/1000$ and $dz_{\min}=1/2000$) detailed in Table II was, thus, chosen to carry out the two-dimensional calculations at $C=2$ and $Re=2000$. The results were compared with those computed at a much refined uniform grid with $h=1/1280$. In Fig. 2(a), no difference is seen between two velocity profiles. As Figs. 2(b) and 2(c), which plot the local flow field along the downstream channel wall, show, Grid-A solution compares fairly well with those computed at $h=1/640$ and $h=1/1280$ in both pressure and vorticity except in the vicinity of the downstream tip corner. This justifies the grid convergence and the use of Grid-A; Grid-A will

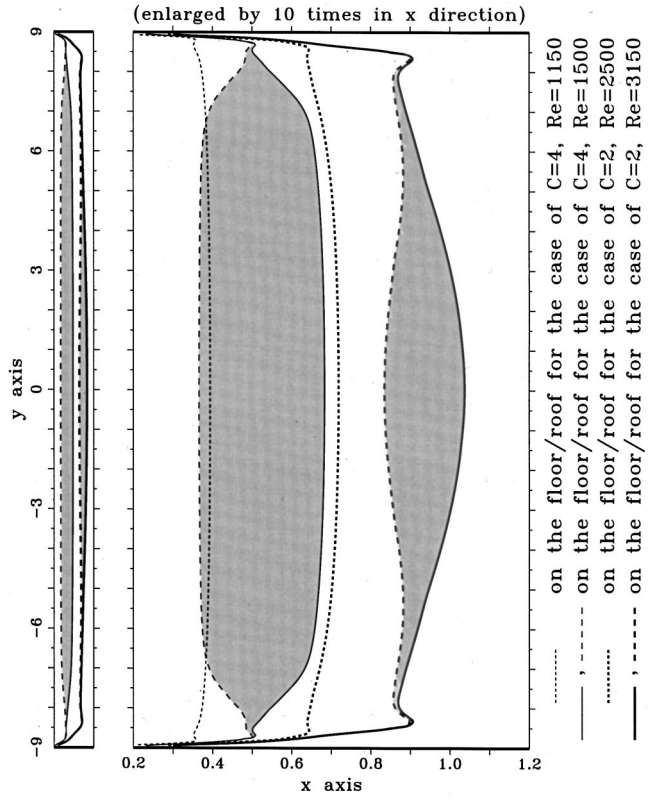

FIG. 13. The spanwise distributions of reattachment length L_3 for the case with $(C,A,Re)=(4,18,1150)$, $(4,18,1500)$, $(2,18,2500)$, and $(2,18,3150)$.

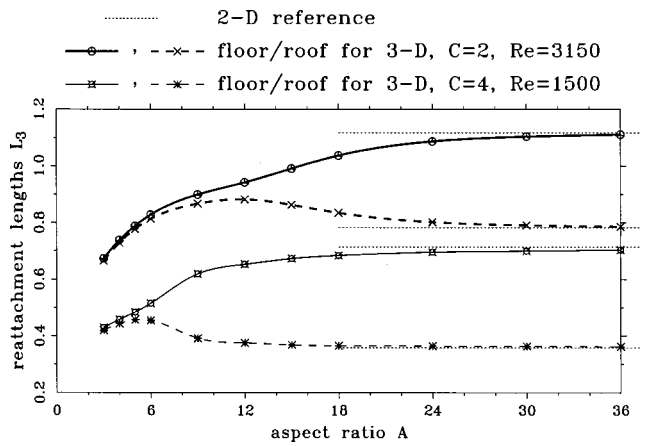

FIG. 14. Reattachment length L_3 on the symmetry-plane $y=0$ of the channel with $C=2$ and $C=4$ for different aspect ratios A.

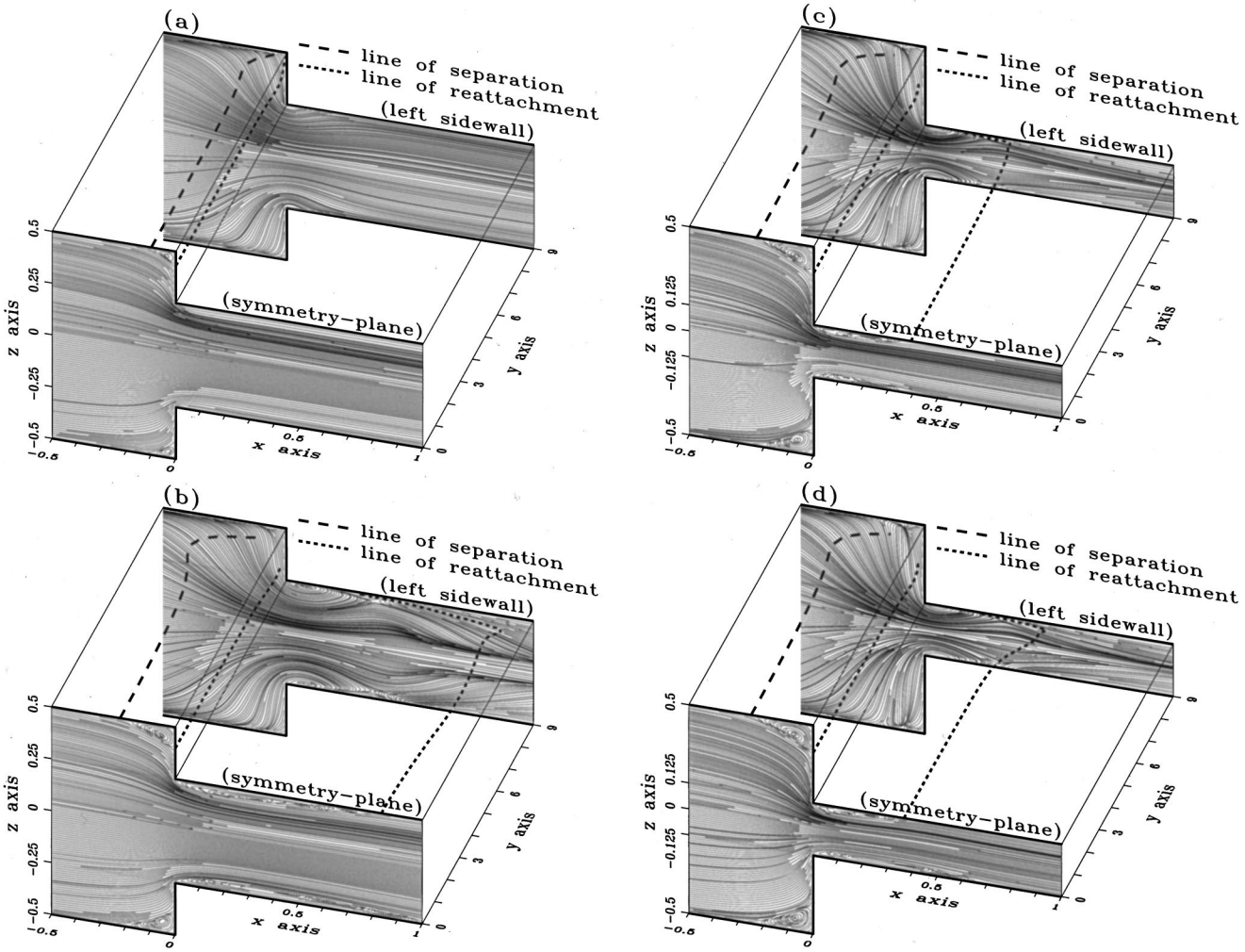

FIG. 15. Plots of lines of separation–reattachment on the channel roof, limiting streamlines on the left sidewall, and, pseudo streamlines on the symmetry-plane $y=0$. (a) $C=2$, $A=18$, and $Re=426$; (b) $C=2$, $A=18$, $Re=3150$; (c) $C=4$, $A=18$, $Re=1150$; (d) $C=4$, $A=18$, $Re=1500$.

be employed in the subsequent three-dimensional study since 99.5% of the grid points can be saved even in the two-dimensional calculation.

The chosen upstream–downstream lengths are 2.5 and 5, which have been used by Hawken *et al.*[5] These lengths are 2 to 3 times those of Durst *et al.*[2] and Huang and Seymour.[6] To study the effect of the upstream–downstream lengths on the flow development, we increased lengths by a factor of 2 and ran the two-dimensional code at $(C,Re)=(2,4000)$ and (4, 2000) on Grid-A. The velocity profiles computed at different channel upstream–downstream lengths agree very well. The computed differences for L_1, L_2 and L_3 are all less than 1%.

For validation purposes, we considered two channels and two flow conditions, $(C=2,Re=426)$ and $(C=4,Re=1150)$, which were previously studied by Durst *et al.*[2] in their experiments. Due to space limitation, we only provide the result for the case of $(C=4,Re=1150)$ here. The interested reader can refer to Sheu *et al.*[25] to obtain the result for the case with $(C=2,Re=426)$. As Fig. 3(a) shows, there is good overall agreement between the computed and experimental data. While a larger discrepancy is observed only in the region immediately upstream of the contraction step, our simulated results have a good agreement with the numerical solution of Durst *et al.*[2] To check whether this discrepancy arises from the nonuniformity of grid, we compare in Fig. 3(b) the results obtained at the nonuniform Grid-A ($dx_{\min}=1/1000$ and $dz_{\min}=1/2000$) with that obtained at the uniform grid with $h=1/1280$. It is found that the agreement is excellent. For providing evidence of insuring the correctness of the present computation, we present in Fig. 4 the comparison of the vorticity distribution of our result with those of the stream function-vorticity formulation,[3,4,6] used together with the Moffatt solution (Moffatt[26]) as an approximation near the downstream tip corner. Figure 4 shows that Grid-A solution compares fairly well with that computed at $h=1/1280$ and has a good agreement with the other referenced data. For further making sure that our code is applicable to solve for the channel flow problem, we have tested the three-dimensional (3D) expansion channel flow problem (Chiang *et al.*[27,28]). Good agreement with the experimental data of Fearn *et al.*[11] makes us to have additional confidence of using the presently computed solution in the subsequent discussion of results.

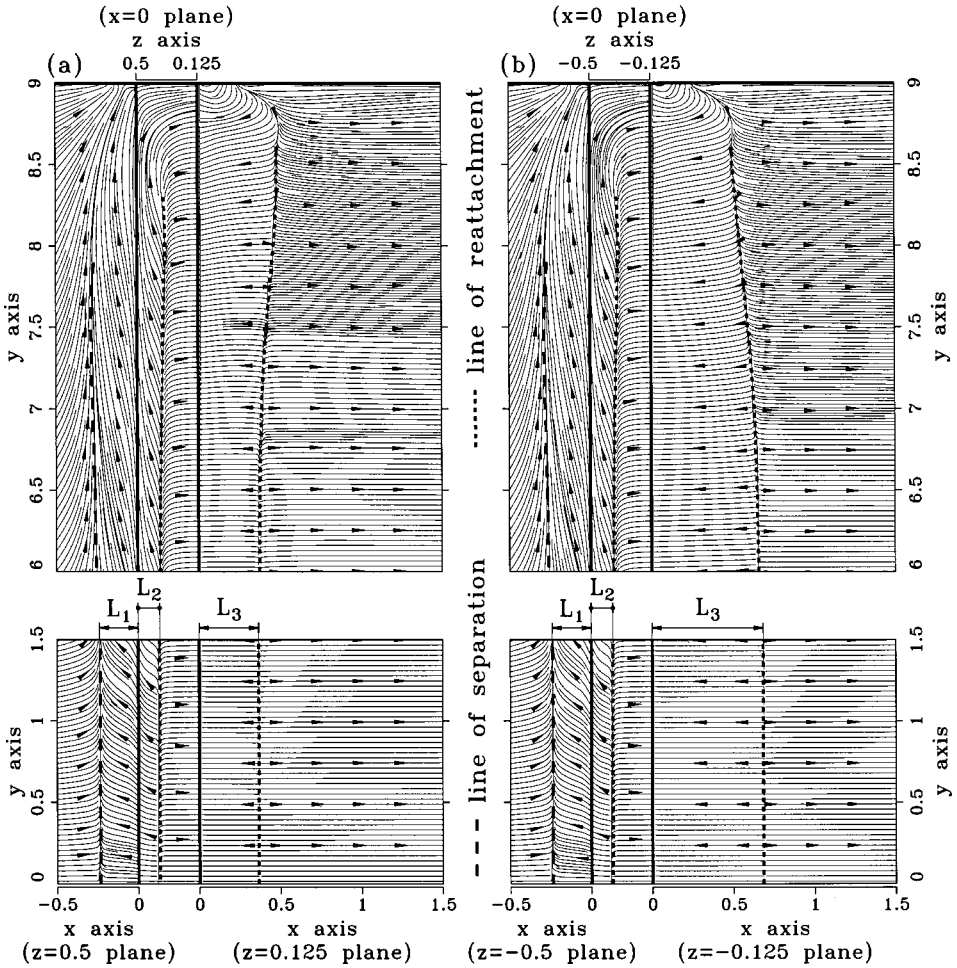

FIG. 16. Lines of separation and reattachment on the channel floor–roof for the case with $C=4$ $A=18$, and $Re=1500$. (a) Limiting streamlines on the channel roof; (b) limiting streamlines on the channel floor.

V. NUMERICAL RESULTS

Having verified the applicability of the proposed finite-volume code to simulate Navier–Stokes flows in the suddenly contracted channel, we will discuss three-dimensional results computed at two sets of C ($=2$ and 4) and five Reynolds numbers, Re ($=426$, 1150, 1500, 2500, and 3150). Discussion of the results will be divided into four subsections.

A. Effects of the channel contraction

In the approach to planar contraction, fluid flow accelerates due to the suddenly decreased channel height. This is followed by a further flow acceleration due to eddies formed immediately downstream of the channel tip. At the streamwise location where the tip eddy forms, the flow experiences an expansion and, thus, decelerates. The flow finally develops into an accelerating mode as it approaches to the channel outlet, with the magnitude of this accelerating velocity being considerably decreased. This accelerating–decelerating phenomenon is best depicted by the pressure contours plotted at the plane of symmetry, $y=0$. For the case of $C=4$ and $Re=1150$, the pressure contour, as shown in Fig. 5(a), in regions upstream of the contraction step bends towards the upstream side. Immediately downstream of the planar contraction step, the pressure contour bends towards the downstream end. This is followed by the emergence of a gradual uniform pressure pattern. Finally, the pressure contour, as expected, turns out to be a nearly vertical straight line ($\partial p/\partial z \approx 0$). Across the contraction plane, the pressure curves are seen to behave as the Moffatt result.[26] Figure 5(b) shows that the pressure continues to decrease to its minimum value at $x=0.17$ and has a sudden drop at $x=0$ along lines $z=0$ and $z=\pm 0.125$, respectively. This is followed by a gradual increase to the local maximum value at $x=0.7$. Downstream of $x=1$, the pressure profile seems to be a nearly straight line ($\partial p/\partial x \approx$ constant). Due to the decrease in the channel cross-section area, the velocity increases by an approximate factor of the contraction ratio if the channel width is sufficiently large.

The flow in the contracted channel section is featured by a fairly uniform core flow and an overshooting boundary layer. Downstream of the contraction step, it is interesting to note that the peak streamwise velocity does not occur at the centerline of the channel. Take the case of $C=4$ as an example; an overshooting velocity profile $u(z)$ at the plane $y=0$ can be observed for $Re=1150$, as seen in Fig. 6(a), owing to flow separation from the channel roof and floor. In light of the conservation of mass principle, the flow velocity must be increased in regions near the flow separation. This overshooting velocity diminishes as the flow gradually develops into the fully developed profile. While $u(y)$ at $z=0$ looks like a uniform core flow, the above mentioned overshooting phenomenon is not seen in Fig. 6(b).

We will next consider the end-wall induced spanwise flow motion in channels having a planar contraction. Figure 6(b) shows that $\partial u/\partial x$ near the sidewall boundary layer has a value larger than that in the core region. This accompanies a negative pressure gradient and, thus, the flow moves towards the two vertical sidewalls. To confirm this, we plot contours of v at a streamwise plane $x=-0.5$. As Fig. 7 shows, the spanwise flow motion is revealed by the movement of fluid particles to the vertical sidewall.

B. Eddy size and pitchfork bifurcation

The suddenly contracted channel flow manifests itself by the presence of re-circulating eddies. An effective means of determining these eddy sizes is, therefore, needed. In this study, we adopted the topological theory (Legendre[29] and Lighthill).[30] Among the available vector fields, we chose limiting streamlines in the present three-dimensional topological study. Limiting streamlines are, by definition, streamlines immediately above the solid wall.[29] Take the case with $(C,Re)=(2,2500)$ as an example; we can theoretically determine lines of separation and reattachment on the channel roof from the limiting streamlines plotted in Fig. 8. This, in turn, enables us to determine three typical lengths L_1, L_2, and L_3, schematically shown in Fig. 1.

Whether or not flow bifurcation of the pitchfork type occurs depends on the channel contraction ratio as well as on the Reynolds number. Based on our previous two-dimensional results[7] shown in Fig. 9, the critical Reynolds numbers beyond which flow started to exhibit bifurcation solutions were determined as 3080 and 1350 for $C=2$ and 4, respectively. With reference to these critical values, we considered Reynolds numbers, tabulated in Table III, in the present three-dimensional studies. It was found that solutions reveal unequal roof–floor eddy sizes as the Reynolds number exceeded its critical value. The evidence is given in Fig. 10, which plots *u*-*w* pseudo streamlines and the *u*-velocity profile at the plane of symmetry, $y=0$, for cases characterized by $(C,Re)=(2,3150)$ and $(4,1500)$. Figure 10 also shows that the reattachment lengths $L_3|_{\text{roof}}$ and $L_3|_{\text{floor}}$ are substantially different. It is the symmetric flow state in the channel that may lose its stability and transit to a stable asymmetric state. The circulating eddies formed immediately downstream of the contraction plane no longer can be symmetric with respect to the symmetry plane $z=0$. Unlike the downstream reattachment length, the upstream separation length L_1 and reattachment length L_2 on the channel roof remain the same as those at the channel floor. This observation is true over all the investigated test conditions detailed in Table III, which tabulates L_1, L_2, and L_3 obtained at the plane of symmetry, $y=0$. The maximum differences for $L_1|_{\text{roof}}-L_1|_{\text{floor}}$ and $L_2|_{\text{roof}}-L_2|_{\text{floor}}$ are found to be less than 1%. To show that such a pitchfork bifurcating flow is physically relevant and is not numerically produced, we perturbed the solutions by an amount of 10 to 20 percentage for the cases studied at $(C,Re)=(2,3150)$ and $(4,1500)$. Both solutions obtained under the stringent convergence criteria mentioned earlier are seen to produce their original bifurcation solutions, implying that it is possible to have the three-dimensional pitchfork bifurcation flow in the presently investigated planar symmetric sudden-contracted channel.

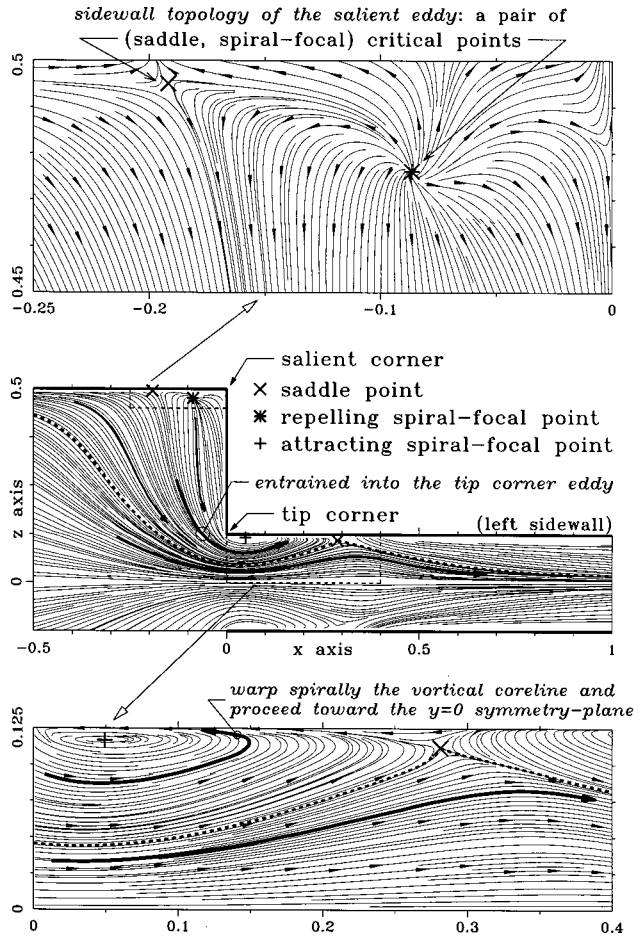

FIG. 17. Topological critical points on the left sidewall, $y=9$ for the case of $C=4$, $A=18$, and $Re=1500$.

The flow at $Re=3150$ can no longer be configured symmetrically with respect to $z=0$ in the channel with $C=2$. Under these circumstances, the pressure plotted in Fig. 11(a) exhibits no *z*-symmetry contours in response to the asymmetric velocity profile shown in Fig. 10(a). To gain deeper insight into the pitchfork bifurcation flow, we plot the velocity and pressure profiles at $x=0.25$ in Figs. 11(b) and 11(c). Of the two downstream tip eddies, the roof eddy has a shorter length L_3 and a larger velocity than those of the floor eddy. On the other hand, a larger pressure value is observed in the floor eddy. Also, a larger pressure gradient is found in the roof eddy. The differences in pressure and velocity are gradually reduced in the approach to $z=0$.

Table III indicates an indication of which flow exhibits pitchfork bifurcation for two channels with $(A,C)=(18,2)$ and $(18,4)$. It has been known for quite some time that the experimentally observed bifurcation is triggered by even a small asymmetry in the channel geometry and inlet flow conditions. In contrast, we attribute the predicted asymmetric solutions in a geometrically symmetric channel flow, subject to a perfect symmetric inlet flow condition, to bifurcation triggered, possibly, by the asymmetric discretization errors and/or asymmetry in the direction-biased numerical algo-

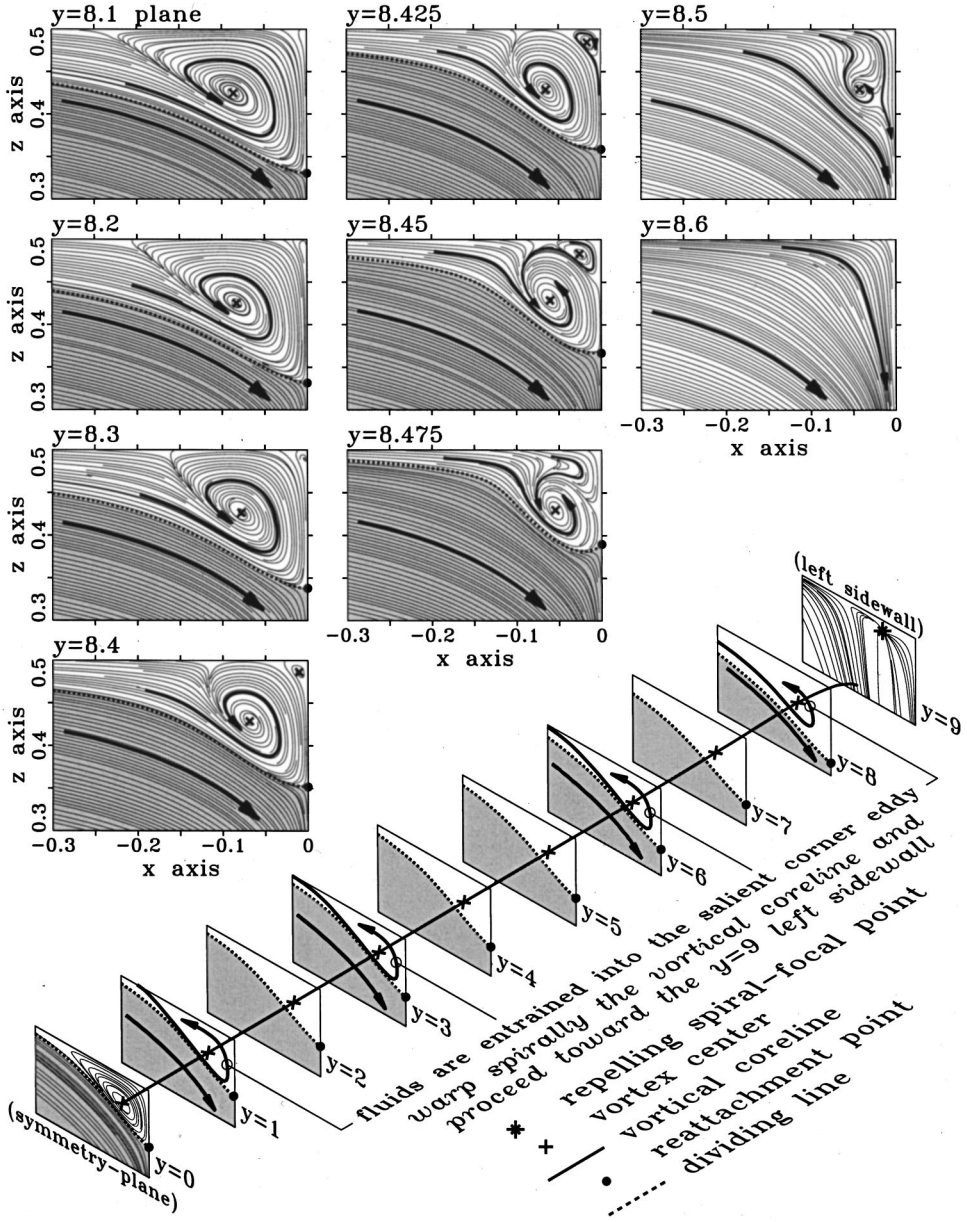

FIG. 18. Spanwise spiral flow of the upstream salient eddy for the case with $C=4$, $A=18$, and $Re=1500$.

rithm employed in the present flow calculation. Another source leading to flow asymmetry is the machine round-off error. On any computer platform, the difference in gap (or spacing) between two consecutive floating-point numbers varies in size. Even a negligibly small machine error may result in flow asymmetry, and this error can be amplified by a locally high shear strain, as seen in Fig. 12, in the vicinity of the step corner.

Figure 13, which has been enlarged 10 times in the x direction for illustrative purposes, plots the spanwise distribution of L_3 for all the investigated Re and C. It is apparent that L_3 is proportional to Re but has little relevance to the contraction ratio. It is also found that $L_3(y)$ is symmetric about $y=0$, indicating that no spanwise mode of the pitchfork bifurcation[28] exists. This is not the case along the step-height direction. In the cases of $(C,Re)=(2,3150)$ and $(4, 1500)$, the difference in $L_3|_{\text{roof}}-L_3|_{\text{floor}}$ is a function of y, and its value is much larger than zero. The bifurcated solution is particularly pronounced and is spatially dependent in the core region $|y|\leqslant 6$. Also clearly revealed by this figure is that the degree of asymmetry decreases as the sidewall is approached.

It has been shown that a decrease in channel aspect ratio has a stabilizing effect.[8] The smaller the channel span width is, the easier the asymmetric flow can be suppressed. This phenomenon has been observed experimentally by Cherdron *et al.*[8] and simulated numerically by Chiang *et al.*,[27] and Schreck and Schäfer[31] in their analyses of planar symmetric sudden expansion flows. In the present study, it is found from Fig. 14 that flow bifurcation can be significantly suppressed as the aspect ratio is reduced to 12 in the channel with $C=2$ $(Re=3150)$ and 6 in the channel with $C=4$ $(Re=1150)$, respectively. As a result, the sidewall can be considered as an aiding factor in suppressing flow bifurcation.

C. Flow topology

When performing a three-dimensional flow simulation, we are often faced with the tedious task of managing a large amount of data. Care must be appropriately taken in order to extract meaningful flow physics and then obtain a profound understanding of the flow structure. In the literature, it is found that we can conduct a theoretically rigorous topological study on limiting streamlines[29] or skin-friction lines[30] to achieve this goal. In this study, the method that exploits limiting streamlines was chosen to gain physical insight into the pertinent fluid flow. Limiting streamlines are, by definition, streamlines passing very close to the wall surface. As the topological theory states, limiting streamlines, as shown in Fig. 8, tend to diverge from lines of attachment. The opposite of lines of attachment are lines of separation. To lines of separation, neighboring limiting streamlines tend to converge. We make use of the kinematic nature of limiting streamlines to classify singular points, such as nodes, foci, and saddles, which enable us to depict the flow structure inferred from the three-dimensional data.

The first step in presenting a global picture of the channel flow was to plot limiting streamlines and lines of separation/reattachment at the channel roof, floor and vertical sidewalls and pseudo streamlines at the plane of symmetry $y=0$ for the investigated flow conditions. Except the case with $Re=426$ and $C=2$, salient and tip eddies can be clearly seen in the region of $|y|\leqslant 8$. These eddies became increasingly less apparent in the rest of the spanwise range, as seen in Fig. 15. The flow near the sidewall is featured by a diminishing spiral flow motion. The spiraling salient eddy passes over the contraction step and, finally, terminates at the spiral-focal point. As for the downstream tip eddy, its motion towards the sidewall is still featured by a less apparent spiraling motion. It is also worth noting that the sidewall streamlines differ considerably from streamlines at the plane of symmetry $y=0$. Figure 15 reveals limiting streamlines of the convergence–divergence–convergence type at the vertical sidewall. This flow complexity is the result of a sudden change in the channel cross section and the increasingly dominant viscous effect near the no-slip sidewall.

Having depicted the flow topology, we plotted the limiting streamlines on the channel roof and floor. Take the case with $C=4$ and $Re=1500$ as an illustrative example. Lines of reattachment and separation, which are used to characterize the spanwise sizes $L_1(y)$, $L_2(y)$ and $L_3(y)$ of the salient as well as the tip eddies, are plotted in Fig. 16. Upstream of the planar step at $x=0$, limiting streamlines bend towards the vertical sidewall such that lines of separation are seen at the channel floor and roof. It is apparent that the spanwise motion prevails inside the upstream salient eddy. The reason for the movement of the fluid particles towards the vertical sidewall is a sudden decrease in the channel cross-section area. Near the sidewall, say $|y|\geqslant 8$, particles inside the downstream tip eddy are seen to repel from the sidewall. In the spanwise range of $|y|\leqslant 8$, clearly seen is a tip eddy, which is reattached to the channel floor or roof. In the core region, the spanwise velocity is so small that the flow is essentially two-dimensional. Of two eddies which form near the contraction

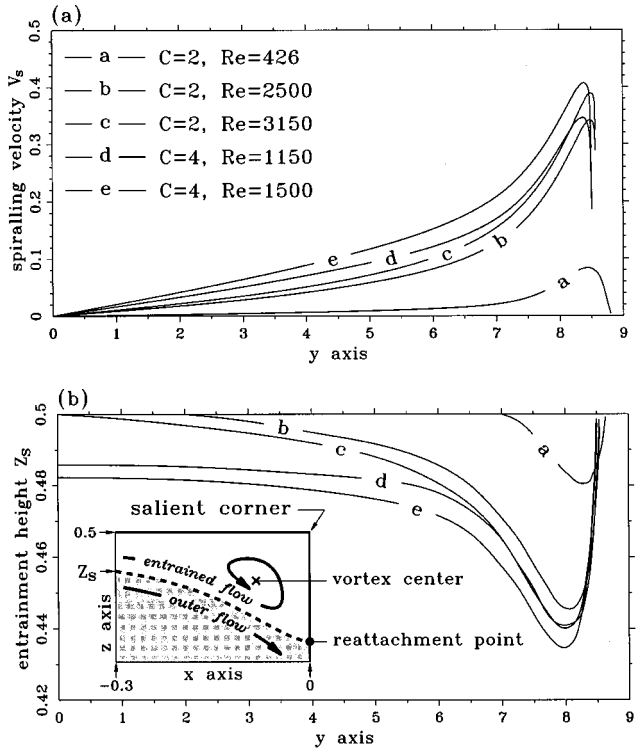

FIG. 19. (a) The distribution of the velocity, which is tangential to the vortical coreline of the upstream salient corner eddy; (b) plot of the entrainment heights of the upstream salient corner eddy against the spanwise coordinates.

step, the flow inside the upstream salient eddy shows an apparent spanwise motion, as compared to that in the downstream tip eddy. This implies that the upstream eddy exhibits a three-dimensional spiraling flow feature.

We then explored the contraction channel flow by sketching the sidewall limiting streamlines. Take the left sidewall as an example; we plot in Fig. 17 limiting streamlines on the plane which is immediately adjacent to the plane $y=9$ for the case with $C=4$ and $Re=1500$. One noteworthy feature of the sidewall limiting streamlines is the formation of two pairs of singular points. These topologically singular points can be classified as saddles and nodal points. Saddle points are defined as having two real eigenvalues of different signs. The limiting streamlines approach the saddle point along the negative eigendirection while they recede along the positive eigendirection. Nodal points (or regular nodal points) are defined as having the real eigenvalues of the same sign. These singular points can be further divided into attracting and repelling types. Attracting nodes are associated with the negative real eigenvalue, and repelling nodes do the reverse. Foci (or spiral-focal points) are also referred to as singular points, whose eigenvalues are, on the other hand, conjugate complex. Depending on the sign of the real part of the eigenvalue, adjacent limiting streamlines spiral either in or out of the singular point.

Following the above topological classification, it is found that each pair of singular points contains a saddle point and a spiral-focal point. One pair of critical points is seen in the upstream salient eddy, and the other is observed at the downstream tip eddy. Owing to the sign of the span-

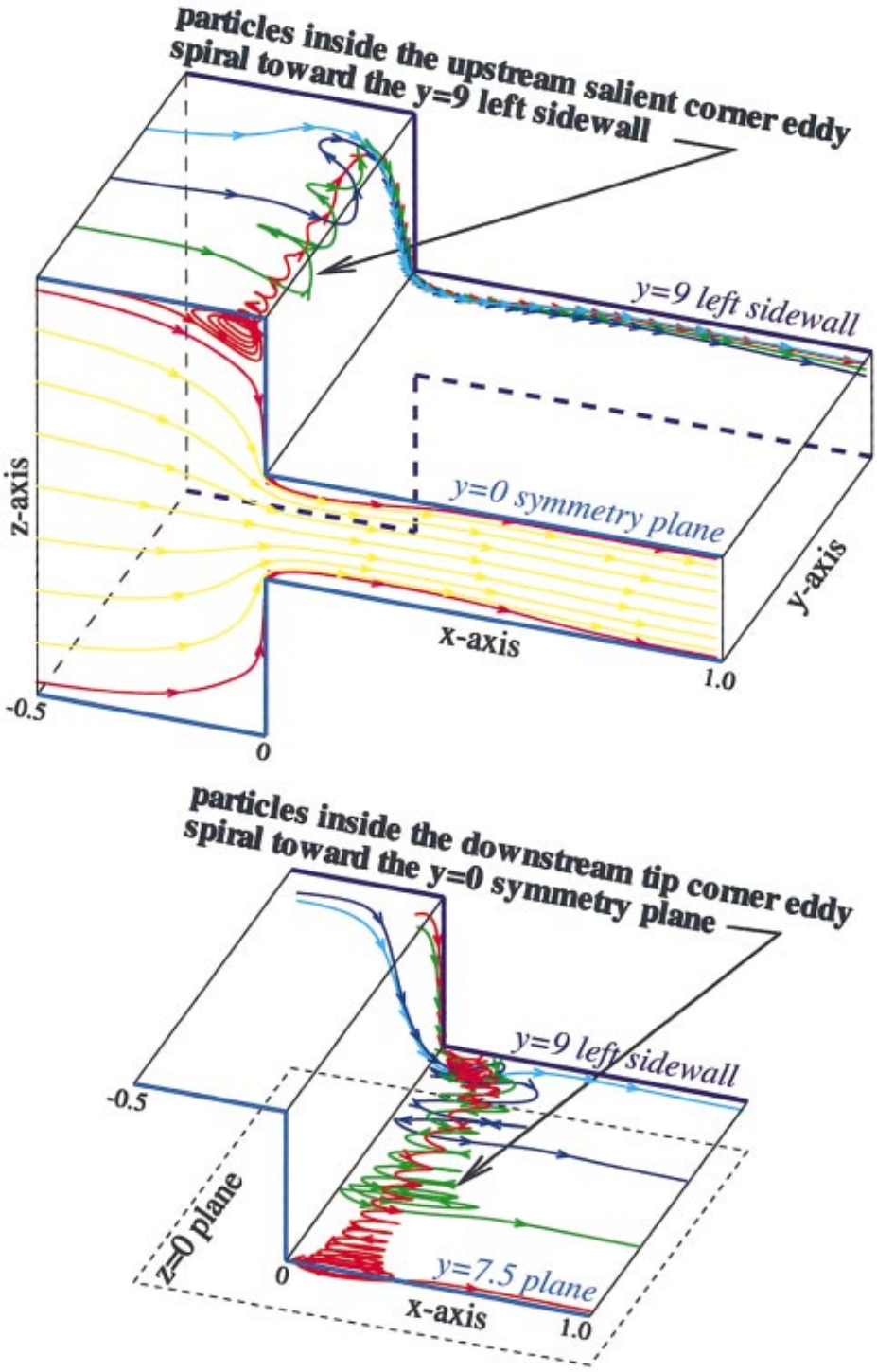

FIG. 20. (Color) Particle tracers for the case with $C=4$, $A=18$, and $Re=1500$.

wise flow velocity upstream and downstream of the contraction planar step, the upstream spiral-focal point is of the repelling type since particles spiral towards the vertical sidewall. All the particles spiral towards the sidewall and, finally, reach this singular point, from which particles repel. In the downstream tip eddy, a saddle point forms along with an attracting spiral-focal point (Sheu *et al.*[32]). Fluid particles adjacent to the focal point spiral towards it and then proceed towards the plane of symmetry $y=0$, as seen in Fig. 16.

D. Spiraling flow structure inside the salient and tip eddies

The three-dimensional suddenly contracted channel flow is manifested by a spanwise motion. This spanwise motion, subject to the primary x-z plane motion, makes the flow three-dimensional and spiraling, especially in the upstream salient eddy and in the downstream tip eddy. We reveal the flow in the upstream salient eddy by showing the spiraling motion in Fig. 18 for the case with $C=4$ and $Re=1500$.

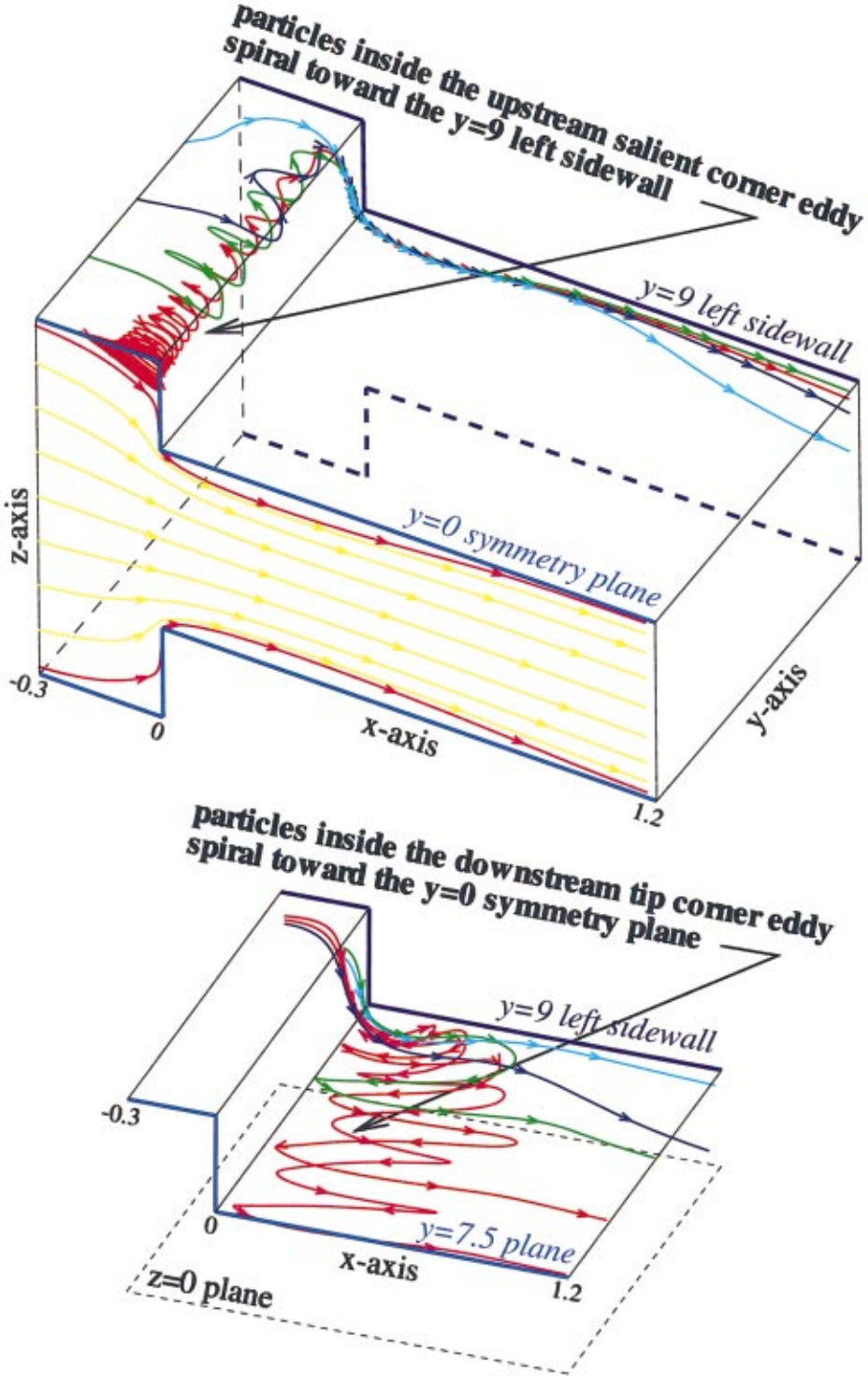

FIG. 21. (Color) Particle tracers for the case with $C=2$, $A=18$, and $Re=3150$.

Clearly revealed by this figure is a vortical coreline inside the salient corner eddy. Particles spiral towards the vertical sidewall along the vortical coreline. The salient corner eddy is of the open type. The upstream fluid particles can be entrained into the salient corner eddy. This is followed by a spanwise spiral motion proceeding towards the two sidewalls. Figure 19(a) reveals that the velocity tangential to the vortical coreline increases its magnitude monotonically from that at the plane of symmetry. The peak value is found at the spanwise location, which is fairly close to the sidewall. Beyond $y=8.5$, this tangential velocity magnitude sharply decreases to zero. It is interesting to note that the location where the velocities tangential to the vortical coreline reaches its peak value is where the corner eddy diminishes. Referring to Fig. 18, a weak pair of unequally sized counter-rotating vortices occurs at the $y=8.3$ plane. In the approach to the two sidewalls, the vortex pair has an increasingly equal vortex size and the vortices can cancel each other out. This leads to a diminishing eddy in the salient corner at the planes $y>8.5$. As alluded to earlier, the salient corner eddy is

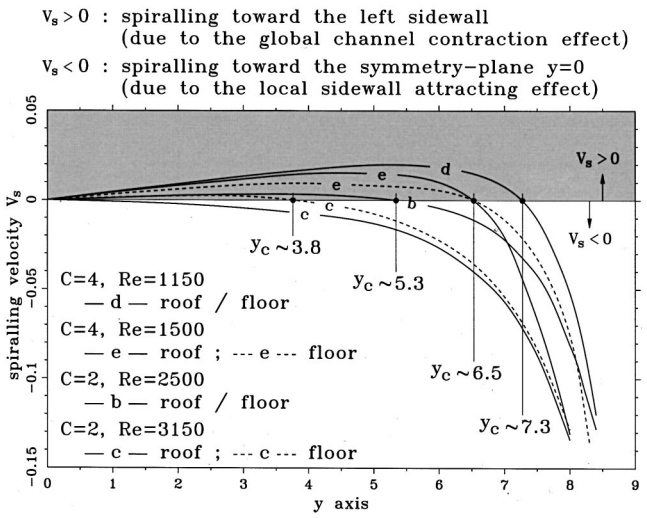

FIG. 22. The distribution of the velocity, which is tangential to the vortical coreline of the downstream tip corner eddy.

not of the close type, so the upstream flow can be entrained into the corner eddy. The height of such an open-type eddy, z_s, schematically shown in Fig. 19(b), was plotted against the spanwise coordinate y. Surprisingly, Fig. 19(b) shows that z_s increases monotonically in the direction towards the vertical sidewall. It is found that at the spanwise location where z_s reaches its peak value, the velocity in the direction tangential to the vortical coreline also reaches its maximum value.

We then discussed spiraling flow motion in the corner eddy by varying C and Re. For all the investigated cases, they vary in a manner similar to that found in the case with $Re=1500$ and $C=4$. The effects of C and Re are best revealed by Figs. 19(a) and 19(b) for the readers' reference. The spanwise spiraling motions in the upstream salient eddy and the downstream tip eddy are best shown by the particle motions in Figs. 20 and 21 for the cases with $(C,Re)=(4,1500)$ and $(2,3150)$, respectively. These plots were obtained by tracing massless particles seeded upstream of the planar step. Particles that are fairly close to the sidewall ($|y|>8.9$) in the upstream salient corner tend to be entrained into the downstream tip eddy and to proceed towards the attracting spiral-focal point shown in Fig. 17. These entrained particles show a spiraling-type motion in their approach to the plane of symmetry. Unlike the particles inside the upstream salient corner eddy, the particles in the downstream tip eddy partly spiral towards the plane of symmetry $y=0$ due to the local sidewall entrainment effect and partly move towards the sidewall due to the global contraction effect.

As noted before, we can construct the vortical coreline inside the downstream tip eddy and, thus, interpolate the velocity component that is tangential to the vortical coreline. As alluded to earlier, these tangential velocities do not all have the same sign. To distinguish the signs of these tangential velocities, we plot v_s in Fig. 22 for all the investigated cases.

VI. CONCLUDING REMARKS

Computational investigations into the flow development in two channels with contraction ratios of 2 and 4 have been performed. This paper has reported results of simulations performed at five Reynolds numbers, 426, 1150, 1500, 2500, and 3150, in order to partly reproduce the existing experimental data and to demonstrate the presence of pitchfork bifurcation solutions. In this study, a line of separation on the upstream channel roof–floor and lines of reattachment on the step plane and on the downstream channel roof–floor have been theoretically determined. Results reveal that the fluid particle inside the upstream salient corner eddy has a tendency to move towards the vertical sidewall. In the upstream salient corner, very few particles in regions fairly close to the sidewall are entrained into the downstream spiral-focal point. Particles inside the tip eddy then spiral towards the plane of symmetry $y=0$. Depending on the values of the channel contraction ratio and the Reynolds number, some of the particles inside the downstream tip eddy spiral towards the plane of symmetry $y=0$, and some of them move towards the vertical sidewalls. Along the upstream and downstream vortical corelines, the location at which the velocity reaches its maximum value is approximately where the location where the vortex diminishes. The sidewall topologies downstream and upstream of the planar step have one feature in common: each of them has a pair of (saddle, spiral-focal) critical points. The difference is that on the upstream side, the spiral-focal point is of the repelling type while on the downstream side it is of the attracting type.

ACKNOWLEDGMENT

This study was supported financially by the National Science Council, Republic of China, under Grant No. NSC 90-2611-E-002-017.

[1] M. J. Crochet, A. R. Davies, and K. Walters, *Numerical Simulation of Non-Newtonian Flow*, Rheology Ser., Vol. 1 (Elsevier, New York, 1984).
[2] F. Durst, W. F. Schierholz, and A. M. Wunderlich, "Experimental and numerical investigation of plane duct flows with sudden contraction," Trans. ASME, J. Fluid Eng. **109**, 376 (1987).
[3] S. C. R. Dennis and F. T. Smith, "Steady flow through a channel with a symmetrical constriction in the form of a step," Proc. R. Soc. London, Ser. A **372**, 393 (1980).
[4] R. Hunt, "The numerical solution of the laminar flow in a constricted channel at moderately high Reynolds number using Newton iteration," Int. J. Numer. Methods Fluids **11**, 247 (1990).
[5] D. M. Hawken, P. Townsend, and M. F. Webster, "Numerical simulation of viscous flows in channels with a step," Comput. Fluids **20**, 59 (1991).
[6] H. Huang and B. R. Seymour, "A finite difference method for flow in a constricted channel," Comput. Fluids **24**, 153 (1995).
[7] T. P. Chiang and T. W. H. Sheu, "Bifurcations of flow through plane symmetric channel contraction," Trans. ASME, J. Fluid Eng. (to be published).
[8] W. Cherdron, F. Durst, and J. H. Whitelaw, "Asymmetric flows and instabilities in symmetric ducts with sudden expansions," J. Fluid Mech. **84**, 13 (1978).
[9] I. J. Sobey, "Observation of waves during oscillatory channel flow," J. Fluid Mech. **151**, 395 (1985).
[10] R. Wille and H. Fernholz, "Report on the first European Mechanics Colloquium, on the Coanda effect," J. Fluid Mech. **23**, 801 (1965).
[11] R. M. Fearn, T. Mullin, and K. A. Cliffe, "Nonlinear flow phenomena in a symmetric sudden expansion," J. Fluid Mech. **211**, 595 (1990).
[12] D. Drikakis, "Bifurcation phenomena in incompressible sudden expansion flows," Phys. Fluids **9**, 76 (1997).

[13]F. Battaglia, S. J. Tavener, A. K. Kulkarni, and C. L. Merkle, ''Bifurcation of low Reynolds number flows in symmetric channels,'' AIAA J. **35**, 99 (1997).
[14]N. Alleborn, K. Nandakumar, H. Raszillier, and F. Durst, ''Further contributions on the two-dimensional flow in a sudden expansion,'' J. Fluid Mech. **330**, 169 (1997).
[15]Z. Rusak and T. Hawa, ''A weakly nonlinear analysis of the dynamics of a viscous flow in a symmetric channel with a sudden expansion,'' Phys. Fluids **11**, 3629 (1999).
[16]J. Mizushima and Y. Shiotani, ''Structural instability of the bifurcation diagram for two-dimensional flow in a channel with a sudden expansion,'' J. Fluid Mech. **420**, 131 (2000).
[17]T. Hawa and Z. Rusak, ''Viscous flow in a slightly asymmetric channel with a sudden expansion,'' Phys. Fluids **12**, 2257 (2000).
[18]T. Hawa and Z. Rusak, ''The dynamics of a laminar flow in a symmetric channel with a sudden expansion,'' J. Fluid Mech. **436**, 283 (2001).
[19]O. A. Ladyzhenskaya, *Mathematical Problems in the Dynamics of a Viscous Incompressible Flow* (Gordon & Breach, New York, 1963).
[20]B. P. Leonard, ''A stable and accurate convective modeling procedure based on quadratic upstream interpolation,'' Comput. Methods Appl. Mech. Eng. **19**, 59 (1979).
[21]T. P. Chiang, R. R. Hwang, and W. H. Sheu, ''Finite volume analysis of spiral motion in a rectangular lid-driven cavity,'' Int. J. Numer. Methods Fluids **23**, 325 (1996).
[22]J. P. Van Doormaal and G. D. Raithby, ''Enhancements of the SIMPLE method for predicting incompressible fluid flows,'' Numer. Heat Transfer **7**, 147 (1984).
[23]T. P. Chiang and W. H. Sheu, ''Numerical prediction of eddy structure in a shear-driven cavity,'' Comp. Mech. **20**, 379 (1997).
[24]F. M. White, *Viscous Fluid Flow*, 2nd ed. (McGraw-Hill, New York, 1991).
[25]W. H. Sheu, T. P. Chiang, and S. K. Wang, ''Flow details of contraction flows in three-dimensional channels,'' Proceeding of 4th International Symposium on Experimental and Computational Aerothermodynamics of Internal Flows, Vol. 2, Dresden, Germany, 1999, pp. 174–183.
[26]H. K. Moffatt, ''Viscous and resistive eddies near a sharp corner,'' J. Fluid Mech. **18**, 1 (1964).
[27]T. P. Chiang, T. W. H. Sheu, and S. K. Wang, ''Side wall effects on the structure of laminar flow over a plane-symmetric sudden expansion,'' Comput. Fluids **29**, 467 (2000).
[28]T. P. Chiang, T. W. H. Sheu, R. R. Hwang, and A. Sau, ''Spanwise bifurcation in plane symmetric sudden expansion flows.'' Phys. Rev. E **65**, 016306 (2002).
[29]R. Legendre, ''Séparation de courant l'écoulement laminaire tridimensionnel,'' Rech. Aerosp. **54**, 3 (1956).
[30]M. J. Lighthill, ''Attachment and separation in three dimensional flow,'' in *Laminar Boundary Layers*, edited by L. Rosenhead (Oxford University Press, Oxford, 1963), Vol. II, 2.6, pp. 72–82.
[31]E. Schreck and M. Schäfer, ''Numerical study of bifurcation in three-dimensional sudden channel expansions,'' Comput. Fluids **29**, 583 (2000).
[32]T. W. H. Sheu, T. P. Chiang, and S. F. Tsai, ''Vortical structures in channel flows with a backward-facing step,'' Int. J. Turbo Jet-Engines **13**, 277 (1996).